J. Fluid Mech. (1990), *vol.* 219, *pp.* 361–385
Printed in Great Britain

The vortices of two-dimensional turbulence

By JAMES C. McWILLIAMS
Geophysical Turbulence Program, National Center for Atmospheric Research,
PO Box 3000, Boulder, CO 80307, USA

(Received 16 May 1989 and in revised form 20 March 1990)

A solution of decaying two-dimensional turbulence at large Reynolds number is analysed by means of an automated vortex census. The census identifies the flow structures which approximately conform to the idealized shape of an isolated, coherent vortex. It also determines vortex characteristics, such as amplitude, size, radial profile, and deformation from the ideal axisymmetric shape. The distributions of these characteristics within the vortex population are examined, as are their time evolutions. Interpretation of these distributions is made with reference to both the random initial conditions for the solution and the dynamical processes of vortex emergence, survival, and interaction.

1. Introduction

In recent years numerical integrations of fluid equations at high Reynolds number have yielded solutions with highly structured flow fields in many different physical situations generally characterized as turbulent. One can marvel at this manifestation of 'order within disorder' and be fascinated both by the beauty of the patterns and by the challenge such a phenomenon presents to dynamical theory.

In a general conceptual framework, we are concerned with many issues related to these so-called 'coherent structures' or 'coherent vortices' in turbulence: the circumstances of their occurrence; their characteristic spatial structure; the statistical distribution of their properties (abundance, amplitude, size, shape) and its time evolution; the dynamical processes occurring to individual vortices in isolation and among a few neighbouring vortices; and the aggregate dynamical behaviour of structured turbulence.

These topics have been most extensively investigated for two-dimensional turbulence. Two-dimensional turbulence is of interest both because it is relatively accessible to computation since it is of lower dimensionality and because it is believed to be an apt paradigm for anisotropic turbulence in three dimensions under conducive circumstances, such as those for planetary-scale flows (McWilliams 1983). There is a long history of numerical solutions for two-dimensional turbulence, beginning with Lilly (1969). More recently (McWilliams, 1984, 1990*b*; Brachet, Meneguzzi & Sulem 1986; Brachet *et al.* 1988; Benzi *et al.* 1986; Benzi, Patarnello & Santangelo 1988; Babiano *et al.* 1987; Santangelo, Benzi & Legras 1990), it has become apparent that coherent vortices develop spontaneously under all circumstances where advective dynamics are dominant (i.e. where forcing and dissipation are not too strong and where lateral boundaries do not excessively constrain the flow), although there are strong indications of this phenomenon in many of the earlier studies as well (e.g. Fornberg 1978; Basdevant *et al.* 1981).

From these solutions, we know that the characteristic vortex shape is an

axisymmetric vorticity pattern with monotonic radial decrease away from a central extremum (i.e. a vorticity monopole). About this underlying monopole pattern, there also occur transient deformations from axisymmetry and transient vortex aggregations (into dipoles or tripoles), as well as rarer, but more substantial deformations associated with vortex creation and destruction.

Many dynamical processes have been identified as important for coherent vortices in two-dimensional turbulence: among these are amplitude decay and lateral spreading through viscous diffusion; limitations on the class of stable vortex shapes set by barotropic instability (e.g. Rayleigh 1880, and the more recent analysis by Dritschel 1988*a*); translation through mutual advection (e.g. Batchelor 1967, p. 530); rotation of azimuthal asymmetries (e.g. Lamb 1932, pp. 231–232); deformation and enhanced dissipation, possibly to the extent of destroying the vortex, in response to a strain field (e.g. Moore & Saffman 1971; Kida 1981); axisymmetrization of an isolated vorticity patch (i.e. a region with a dominant sign in the vorticity field; e.g. Melander, McWilliams & Zabusky 1987); merger of like-sign vortices (e.g. Christiansen & Zabusky 1973); and aggregation of opposite-sign vorticity extrema into apparently stable, dipole (e.g. Batchelor 1967, p. 535) and tripole (e.g. Leith 1984) configurations. Each of these processes has been investigated under idealized circumstances, with varying degrees of completeness in theoretical understanding, but this literature is much too extensive to survey here. It can be approached either through the references in the numerical studies cited above or in the survey of McWilliams (1990*a*).

As yet there has been relatively little quantitative measurement of the properties specific to the coherent vortices in turbulence, as opposed to more generic (and traditional) flow descriptors such as Fourier spectra and low-order statistical moments of the velocity and vorticity fields. On the other hand, from visualization of these fields (especially vorticity) in numerical solutions, interesting and apt descriptions of vortex properties have been made by the investigators listed above, but mostly these descriptions have been qualitative and subjective in nature. For example, it has been noted that vortices occur with wide ranges in size, amplitude, and radial profile, and that the particular property distributions of the emergent vortices are strongly influenced by the initial conditions or forcing (this is further discussed in §7). However, largely independent of the emergent property distributions, there are subsequent evolutionary tendencies towards fewer, more widely separated vortices, a greater rate of decrease in the number of weaker vortices compared to the rate for stronger vortices, a decay of the amplitude of vorticity extrema, a growth in vortex size, and a decreasing degree of deformation from axisymmetry among the surviving vortices.

At present there is no proper theory for the aggregate dynamics of coherent vortices. It is, however, clear that their presence does strongly influence two-dimensional turbulent cascade rates: the rates of energy transfer to larger spatial scales and of enstrophy transfer to smaller scales, where it is dissipated, are reduced through the capture and retention of vorticity in the coherent vortices on intermediate scales (Basdevant *et al.* 1981; Herring & McWilliams 1985; McWilliams 1990*a*, *b*).

The purposes of this paper are to present a methodology for the quantitative analysis of vortex properties, to illustrate it for a particular solution of weakly decaying two-dimensional turbulence, and to indicate in a qualitative fashion the associations between these properties and vortex dynamics. I view this type of analysis of vortex properties as a probably necessary step towards developing a

satisfactory theory or minimal model of the aggregate dynamics of structured turbulence.

2. The solution

The analysis of vortex properties will be made on a particular numerical solution of two-dimensional turbulence in a high-Reynolds-number regime of weakly decaying energy. Here we briefly describe the solution. (Much more extensive descriptions of similar solutions are in the numerical papers cited in §1.)

The model is the barotropic vorticity equation with hyperviscous diffusion, which is a simple, commonly used parameterization for subgrid-scale vorticity mixing:

$$\zeta_t + \mathrm{J}(\psi, \zeta) = -\nu \nabla^2 \nabla^2 \zeta. \tag{1}$$

Here ζ is the vorticity, and ψ is the stream function. Horizontal velocities u, v are related to them by

$$u = -\psi_y, \quad v = \psi_x, \quad \zeta = v_x - u_y = \nabla^2 \psi. \tag{2}$$

The spatial differential operators J and ∇^2 are the horizontal Jacobian and Laplacian, respectively. The domain is a square of dimension 2π, and the boundary conditions are periodicity.

The initial conditions are a random-phase realization from a kinetic energy spectrum of moderate bandwidth. We define the spectrum $E(k)$ in relation to the total energy such that

$$E = \frac{1}{2}\frac{1}{4\pi^2}\int\int \mathrm{d}x\,\mathrm{d}y(u^2+v^2)$$

$$= \sum_k E(k), \tag{3}$$

where k is the horizontal wavenumber modulus. The summation in (3) is the discrete approximation to a wavenumber integral, with the differential $\mathrm{d}k = 1$. This particular solution was obtained for the initial spectrum shape

$$E(k) \propto \frac{k^6}{(k+2k_0)^{18}}, \tag{4}$$

an amplitude normalization $E(t=0) = 0.5$, a spectrum peak at $k_0 = 30$, a hyperviscosity $\nu = 3.5 \times 10^{-9}$, a spatial grid resolution $\mathrm{d}s = 2\pi/450 = 0.014$, and a temporal resolution $\mathrm{d}t = 0.0025$. The value of k_0 is large compared to $k_{\min} = 1$ so that a large population of vortices emerges in the solution; furthermore, k_0 is small compared with $k_{\max} \approx 225$, so that a hyperdiffusion time, $t_\nu = 1/k_0^4\nu = 350$, is long compared with an initial eddy circulation (i.e. advective) time, $t_c = Z(t=0)^{-\frac{1}{2}} = 0.021$, where Z is the enstrophy (i.e. spatially averaged vorticity variance). The model uses a dealiassed spectral method which is conservative of both E and Z when $\nu = 0$ and $\mathrm{d}t \to 0$ (Orszag 1971); the time integration is by a standard leapfrog scheme.

By now many of the solution properties are familiar. In table 1, we can see that the energy decay is slight (because ν is small), yet the enstrophy decay is substantial. The time of maximum enstrophy dissipation is $t \approx 0.25$, which is approximately a strain-enhanced enstrophy dissipation time, $t_Z = t_c \ln(t_\nu/t_c)$ (NB this is a variant, for hyperviscosity, of the result discussed by Lesieur 1987, p. 194).

t	E	Z	k_ζ	Ku
0	0.500	2229	67	3.0
0.1	0.495	2027	79	3.2
0.2	0.489	1745	81	3.5
0.4	0.479	1274	77	4.0
1.0	0.464	605	61	6.4
2.0	0.457	315	44	12.1
4.0	0.453	184	32	20.6
10.0	0.449	104	24	33.0
20.0	0.447	72	15	43.2
40.0	0.444	53	11	50.0

TABLE 1. Solution properties

Table 1 also includes the vorticity centroid wavenumber,

$$k_\zeta = \frac{\sum\limits_k k^3 E(k)}{\sum\limits_k k^2 E(k)}, \tag{5}$$

which initially increases as enstrophy density (i.e. $k^2E(k)$) is transferred to smaller scales and which subsequently, after the time of maximum dissipation, decreases as enstrophy is dissipated at small scales and the peak in $E(k)$ shifts towards larger scales. Finally, the vorticity kurtosis

$$Ku = \frac{\iint \mathrm{d}x\,\mathrm{d}y\,\zeta^4}{\left(\iint \mathrm{d}x\,\mathrm{d}y\,\zeta^2\right)^2} \tag{6}$$

grows steadily with time (table 1), which indicates an increasing spatial intermittency in the vorticity field due to the emergence of and increasing dominance of the solution by coherent vortices. The vortices are evident in figure 1.

3. Rationale for an automated vortex census

The objective is to analyse numerical solutions of two-dimensional turbulence in order to identify the vortices present and then to measure their properties. The first of these tasks is one of pattern recognition or feature eduction; the second is an important analysis technique for flows dominated by coherent structures.

The identification or selection criteria are based upon a posited archetypal vortex structure: the vorticity field has a single sign in a simply connected region about a single horizontal extremum of significant amplitude (compared to, say, the square root of the enstrophy); furthermore, within this region the pattern is axisymmetric about the extremum. This archetype derives from experience with many solutions of this type, and a vortex with this shape is a steady, stable solution for inviscid, two-dimensional flow in an unbounded domain. (The assertion of axisymmetry would have to be reconsidered for a horizontally non-isotropic flow environment, e.g. with a large-scale shear or a spatially variable Coriolis frequency.) Candidate vortices which deviate excessively from this archetypal structure are rejected.

This simple and spatially smooth vortex shape develops through the process of axisymmetrization of a vorticity patch, which can ensue from either irregular initial

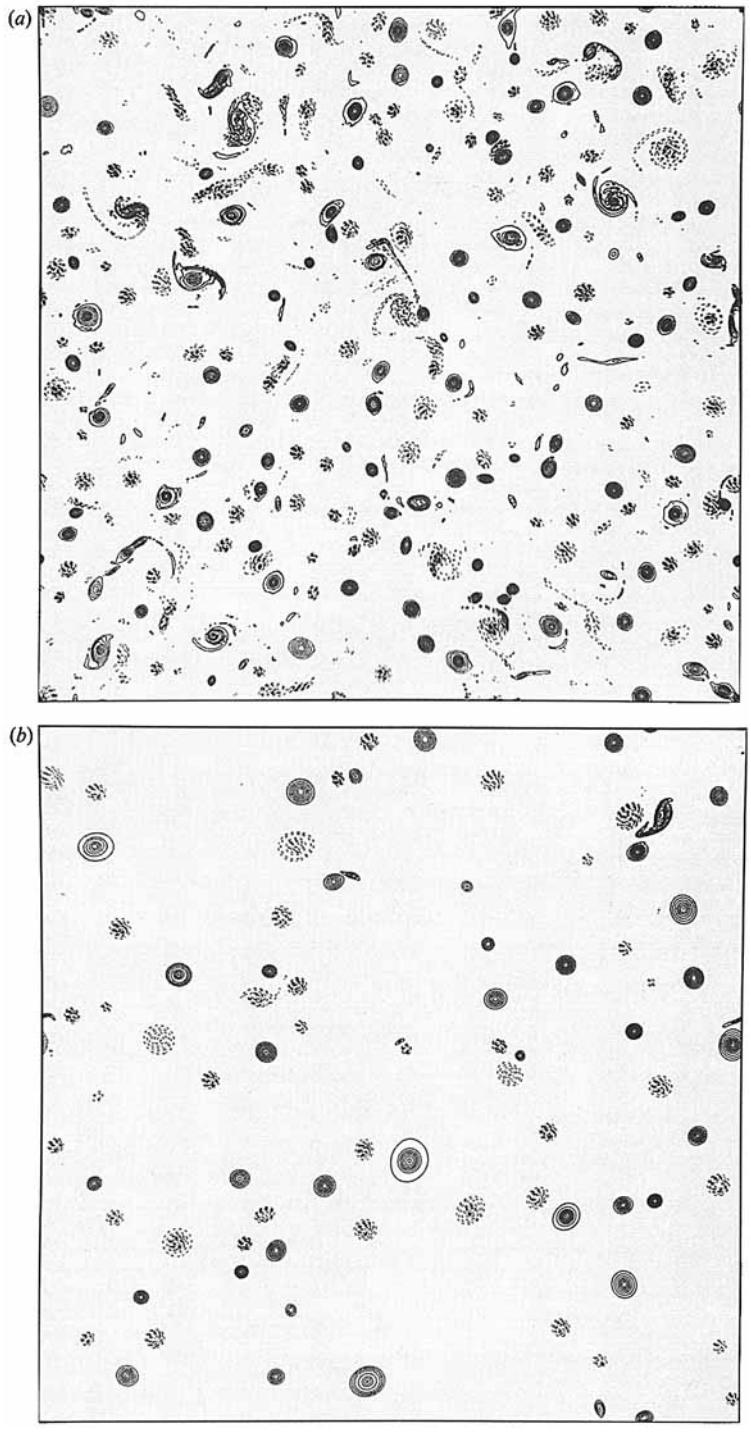

FIGURE 1. $\zeta(x, y)$ at (*a*) $t = 5$ and (*b*) 20. The contour interval is 10. Positive contours are solid, and negative contours are dashed. The zero contour is omitted.

conditions, the subsidence of a deforming strain field associated with neighbouring vorticity patches, or the onset of a merger event. Axisymmetrization, however, is initiated (on a time t_c) by making the patch less smooth with increasing vorticity gradients and elongating vorticity filaments, and smoothness is achieved only through diffusion of the filaments and dissipation of their enstrophy on a time t_Z (Melander *et al.* 1987). Thus our selection criterion based upon smooth vortex shapes is inapt for an axisymmetrizing patch during a time interval between t_c and t_Z, whose ratio is the logarithm of a Reynolds number $Re\,(=t_\nu/t_c)$. In all present turbulence solutions containing many vortices (including the one analysed here), the achievable spatial resolution sufficiently limits the value of Re so that this interval is not too long, and the rejection of a candidate vortex during a non-smooth stage of axisymmetrization is not a serious deficiency of the selection criterion. However, in a hypothetical solution with very large Re, this interval of non-smoothness will be very long, but the non-smoothness is transferred to scales small compared with the patch size within a few t_c, and subsequently we expect it to have no dynamical influence on either the local behaviour of the vortex or the global dynamics of the energetic scales of motion. Thus, the present selection criterion could be generalized for very large Re by being applied to the low-pass-filtered vorticity field on scales comparable with the patch size, but this step is unnecessary for present solutions.

It would be possible to define a less stringent selection criterion. One definition, used by Babiano *et al.* (1987) and Benzi *et al.* (1988), is all regions with vorticity above a small threshold amplitude. Another, due to Weiss (1981) and used by McWilliams (1984), Brachet *et al.* (1988), and Benzi *et al.* (1988), is all regions with a negative sign for the determinant of the velocity gradient. Both of these alternatives are simpler to implement than what is proposed in §4, and the latter one has a plausible dynamical basis. At intermediate times in the solutions, hundreds of $t_c(0)$ units, when the vortices are well developed and widely separated on average, all of these selection criteria yield substantially the same set of vortices. However, at earlier times, these simpler alternative criteria would select either most of the domain or about half of it, respectively, and this would be highly misleading with respect to the dynamical behaviour we associate with coherent vortices. Thus, we prefer more discriminating selection criteria.

It also would be possible to define more stringent selection criteria by testing for additional characteristics. Among the more plausible possibilities are the following: (i) The usual structure for an isolated vortex is monotonic decrease of vorticity with radial distance from a single-point extremum. An argument against testing for this condition is that it is temporarily violated during a vortex merger event before axisymmetrization returns the profile to monotonicity. (ii) Coherent vortices tend to become spatially isolated as the vorticity field between vortices is depleted by a strain-induced cascade (scale transfer) to dissipation and as the number of vortices decreases through non-conservative straining and merger interactions. However, isolation is not an attractive selection criterion since close approaches do intermittently occur through mutual advection among vortices, even when sparse. (iii) Temporal history aids a human analyst in identifying the coherence of a vortex (i.e. time continuity of shape, longevity, dynamical plausibility of events). However, a determination of vortex structure would seem likely to precede an understanding of vortex dynamics, and so the former should not be excessively biased by the latter in a first quantitative census. Alternatively stated, a census obtained without dynamical prejudice allows uncontaminated inferences about dynamical processes.

The essential characteristics of coherence for vortices in turbulence are the

persistence and recurrence of a particular flow pattern (an axisymmetric vorticity monopole) and the longevity of individual vortices compared to the advective evolution times t_c and t_Z. In the census selection criteria, we test for the spatial pattern, but not the longevity.

Thus, there is an inherent tension in the selection process. At one extreme, strict and narrow selection criteria, applied with tight quantitative tolerances between the solution and the archetypal structure, will assure the analyst that only the best vortices are selected. However, many coherent vortices exhibit transient departures from the archetype and thus would be falsely rejected by excessively strict criteria. Furthermore, there is a potential circularity in an overly strict selection analysis: the only information in the outcome would be the number of vortices present, while all their properties would be implicit in their selection criteria. At the other extreme, of course, too few selection criteria, too loosely applied, would select flow structures which a subjective analyst would reject, and inferences about coherent vortex properties would be contaminated by incoherence.

No unambiguous resolution of this tension can be achieved. The particular selection criteria stated above, applied with the tolerances described below, are thus a compromise chosen on the basis of many case studies. Their justification lies in successfully identifying the same coherent vortices as does the human analyst, with the added benefit of explicit criteria consistently applied. I have found the census to be quite successful, in this sense, for strong vortices well after their emergence from random initial conditions, except during some close interactions with strong structural deformations and a high probability of imminent vortex disappearance. On the other hand, weak or incipient vortices are often far from the archetype, and the human analyst can find such selection decisions quite uncertain. The reader must judge the aptness of the census from the *a priori* plausibility of its selection criteria (§4) and the *a posteriori* consistency of its results (§§5 and 6).

4. Vortex selection procedure

Here we specify the procedure to identify vortices in a two-dimensional gridded vorticity field $\zeta(x, y)$ at a particular time.

A. *Identify extrema* Vortices are required to have a two-dimensional extremum in vorticity as their centre, with an amplitude above a specified threshold value.

Procedure Determine the amplitudes ζ_n and positions $(x_n, y_n), n = 1, \ldots, N_e$, for all extrema above a threshold value $\zeta_{\min}$. The extremum test further requires that a candidate extremum have the largest magnitude within a local square of dimension L_e.

Comments A minimum value for L_e is $2\mathrm{d}s$, where $\mathrm{d}s$ is the horizontal grid spacing. In practice, L_e is taken to be $4\mathrm{d}s\,(= 0.0558$ here), since extrema within two grid points of each other are invariably determined to be part of the same vortex by the additional procedures below. The value for $\zeta_{\min}$ is taken to be a small fraction of the global vorticity extrema and is held constant in time, even though the latter decreases by a little more than a factor of two over the approximately $1000t_c$ units of integration (see figure 7 below). For decreasing values of $\zeta_{\min}$, a rapidly increasing fraction of the weakest extremum is rejected as vortices by the tests below; thus the census is not very sensitive to the value of $\zeta_{\min}$. For the present example, with a global vorticity extremum of $\max|\zeta| = 212$ at $t = 0$, we choose $\zeta_{\min} = 10$.

B. *Identity interior and boundary regions* Vortices have a simply connected region with vorticity of the same sign as its central extremum.

Procedure Search away from the central extremum in the $+x$-direction until a vortex boundary is encountered. This is defined as the last point along the search line such that

$$\frac{\zeta}{\zeta_n} \geqslant \Delta. \tag{7}$$

From that first boundary point, we declare $+y$ as the current search direction and trace the vortex boundary along horizontal grid lines in a counterclockwise direction until returning to the first point (a candidate vortex is rejected if the boundary is not a closed curve). The tracing algorithm is the following:

(i) From the current boundary point, test whether the next grid point 90° to the right of the current search direction satisfies (7); if so, then rotate the current search direction 90° to the right, accept this grid point as the new current boundary point, and return to the beginning of (i); if not, then go to (ii).

(ii) Test whether the next grid point in the current search direction satisfies (7); if not, then rotate the search direction by 90° to the left and return to the beginning of (ii); if so, then accept this grid point as the new current boundary point, and return to the beginning of (i).

We denote the ordered set of boundary grid points as δV_n; note that a grid point can enter twice into δV_n if it lies along a protrusion of width 1ds where condition (7) is satisfied. The vortex interior V_n is the set of grid points contained inside or on the closed curve defined by δV_n. If any grid point within V_n fails to satisfy (7), the candidate vortex is rejected.

Comments If Δ is chosen too large, then a substantial portion of the vortex is not included in V_n. If Δ is chosen too small, then the identified boundary is likely to be much more distorted from circular than are typical vorticity contours in the vortex interior. $\Delta = 0.2$ has been found to be a satisfactory value which avoids both perils.

C. *Eliminate redundancy* All independent vortices are spatially separate.

Procedure If any extremum lies within the interior set V_n of another vortex with a stronger extremum, the former is discarded as an independent vortex.

Comments This restriction is usually an appropriate one. However, an exception occurs during a vortex merger event, after the initially separate vortices have become entangled and before the final axisymmetrization is complete. However, because mergers are completed rapidly in the present solutions (see §3), and involve only a small fraction of the vortex population at a time, only a modest underestimate of the vortex population is made by excluding this situation.

D. *Test vortex shape* The vortex interior and boundary should not depart excessively from axisymmetry.

Procedure For each candidate vortex the following shape properties are calculated:

$$C = \sum_{\delta V} \mathrm{d}s, \tag{8}$$

$$A = \sum_{V} \mathrm{d}s^2, \tag{9}$$

$$\delta x_i = \frac{\sum_V \mathrm{d}s^2\, w(x_i - x_{ni})}{\sum_V \mathrm{d}s^2\, w}, \tag{10}$$

$$M_{ij} = \frac{\sum_V \mathrm{d}s^2\, w(x_i - x_{ni})(x_j - x_{nj})}{\sum_V \mathrm{d}s^2\, w}. \tag{11}$$

These quantities are, respectively, the circumference, the area, the first spatial moment or centroid displacement, and the second-moment matrix. i and j are horizontal coordinate indices (i.e. $(x_1, x_2) = (x, y)$), and w is a weighting factor equal to either 1 or ζ. M_{ij} has positive eigenvalues $\lambda_1 \geqslant \lambda_2$.

Using these quantities, the following tests are done:

$$C \leqslant C_{\max}, \tag{12}$$

$$A \leqslant A_{\max}, \tag{13}$$

$$r \equiv (A/\pi)^{\frac{1}{2}} \geqslant r_{\min}, \tag{14}$$

$$R \equiv \frac{C}{2\pi^{\frac{1}{2}} A^{\frac{1}{2}}} \leqslant R_{\max}, \tag{15}$$

$$\delta \equiv \frac{(\delta x_1^2 + \delta x_2^2)^{\frac{1}{2}}}{r} \leqslant \delta_{\max}, \tag{16}$$

$$\epsilon \equiv \left(\frac{\lambda_1}{\lambda_2} - 1\right)^{\frac{1}{2}} \leqslant \epsilon_{\max}. \tag{17}$$

Candidate vortices failing any of these tests are rejected.

Comments Tests (12), (13), and (14) are imposed primarily for computational reasons. Tests (12) and (13) limit the size of the candidate vortex to a modest fraction of the domain size. This limits the computer memory required to conduct the census and, if the tests are failed, avoids the need to do the subsequent tests. As long as the bounds are not too stringent, (12) and (13) do not eliminate any vortices the human analyst would accept. For the present census, we adopt the values $C_{\max} = \frac{1}{4} \times (8\pi) = 6.28$ and $A_{\max} = [0.1 \times (2\pi)]^2 = 0.395$. The radius test (14) is intended to ensure that spatial resolution is not grossly inadequate for any candidate vortex. We therefore choose $r_{\min} = \mathrm{d}s = 0.014$, and find that this test is rarely failed except during the early period of vortex emergence.

Tests (15), (16), and (17) are all limitations on departures from axisymmetry (circularity of vorticity contours). The parameter R in (15) is one for a circular boundary. It is larger than one for all other shapes, and it increases with boundary shape complexity. δ in (16) is the displacement of the vortex centroid from its centre normalized by its radius; it has the value zero for an axisymmetric, monotonic vorticity profile. The eigenvalues of M are equal to one quarter times the squares of the major and minor axes for an elliptical fit to δV with $w = 1$. Hence, ϵ in (17) is the ellipticity of the vortex; it is zero for a circle and positive otherwise. Tests (16) and (17) are made with both choices of w, although $w = 1$ usually provides the more severe test because of radially decreasing vorticity profiles. (For the vortex properties reported below, $w = 1$ unless stated otherwise.) We choose the values $R_{\max} = 1.75$, $\delta_{\max} = 0.35$, and $\epsilon_{\max} = 2.5$. These values are somewhat conservative, in that they exclude a few significantly distorted vortices which the human analyst might accept, particularly where the distortion is known *a posteriori* to be only transient. The fundamental basis for these choices is an empirical one: they approximately represent the boundary that a human analyst would draw between distorted vortices and other, incoherent structures in the vorticity field, as determined by application of these tests to many examples of both. Fortunately, the sensitivity to this boundary is not too great: within a broad range about these values of $(R_{\max}, \delta_{\max}, \epsilon_{\max})$, the number of vortices at the margin of acceptance is a small fraction of the total population.

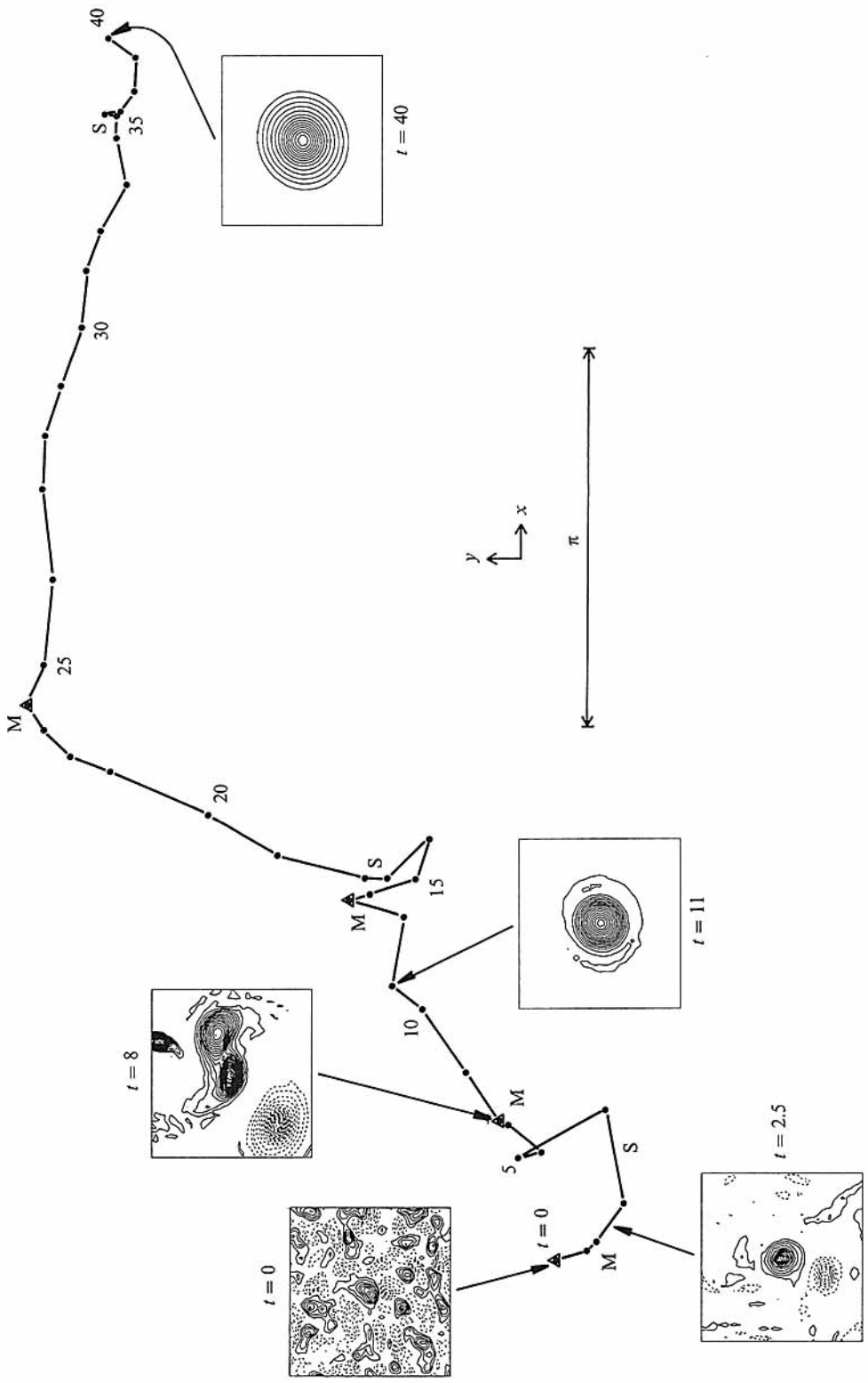

FIGURE 2. For caption see facing page.

After all this, a set of N_v coherent vortices has been selected, and many of their important properties have been determined.

5. Life history of a single vortex

Before examining the vortex population as a whole, we apply the vortex property measures to the life history of a single vortex. It is more interesting to choose a vortex that survives for the entire length of the integration (i.e. until $t = 40$) than one which suffers an early destruction. We choose the vortex with the strongest vorticity extremum at $t = 40$. It can be traced continuously backwards in time to an extremum which is the 28th strongest in the random initial conditions. It occupies an intermediate rank at times in between. Because it is always among the strongest vortices, it has relatively weaker deformations and less vulnerability to destruction in its close interactions with other vortices. If a more typical vortex life history were followed, it would likely be more tumultuous.

The trajectory of the vortex extremum is shown in figure 2, along with indications of its major interaction events, the times at which the selection procedure rejects it, and representative plots of its evolving shape. It can also be seen in figure 1, where its coordinates are (3.36, 0.84) at $t = 5$ and (6.23, 3.46) at $t = 20$. (NB the coordinates span $[0, 2\pi]$). The census is applied at all unit times between 0 and 40, as well as at $t = 0.5$ for better early resolution.

The selection procedure rejects this vortex at $t = 0$ because its normalized centroid displacement is $\delta = 0.41$, which is slightly in excess of δ_{max}. On the other hand, we see in the insert panel in figure 2 that only a modest evolution of the vorticity pattern through the axisymmetrization process would make it a good vortex; indeed, by $t = 0.5$ the selection procedure accepts it. Thereafter, it is selected as a vortex for all times except three (i.e. $t = 8$, 13, and 24) when it is in the midst of mergers with other vortices (NB the $t = 8$ merger is shown in an insert panel in figure 2) and it is rejected for either excessive ϵ or δ or for lack of a simply connected vortex interior V_n.

During the lifetime of this vortex, it undergoes four mergers with other vortices and three major straining interactions, during which it is appreciably deformed and its (weaker) partner is deformed to a greater degree. (An example of a minor straining interaction can be seen in figure 1(*b*), near $(x_n, y_n) = (6.23, 3.46)$, where the quite weak partner is being destroyed by the strain field on the periphery of the vortex.) Interaction events become less frequent as the vortex population becomes sparser.

Histories of some vortex properties are shown in figure 3. The amplitude tends to decrease with time (figure 3*a*), more rapidly early and less rapidly later. This is because of the lessening of the frictional decay rate, owing both to the systematic growth in size of the vortex (figure 3*b*) and to its generally decreasing deformation (figure 3*d*) as the population density declines and close encounters become rarer. The largest decreases in amplitude occur during merger events. Two instances of temporary and slight amplitude growth also occur during mergers; they are due either to numerical error in calculating the Lagrangian conservation of vorticity (i.e.

FIGURE 2. Trajectory of a single vortex. Positions of the extremum are plotted at unit times, and times are labelled every $\Delta t = 5$. A triangle on the trajectory marks a time when the selection procedure rejects the vortex. Events of close vortex interaction are marked beside the trajectory: either merger (M) or strong straining deformation (S). In addition, contour plots of vorticity appear as insert panels at selected times in sub-domains of lateral dimension 0.279 centred on the vortex extremum (i.e. there is a scale magnification of a factor of 5 relative to the trajectory plot); the contour interval is 24 at $t = 0$, 12 at $t = 2.5$, and 6 thereafter.

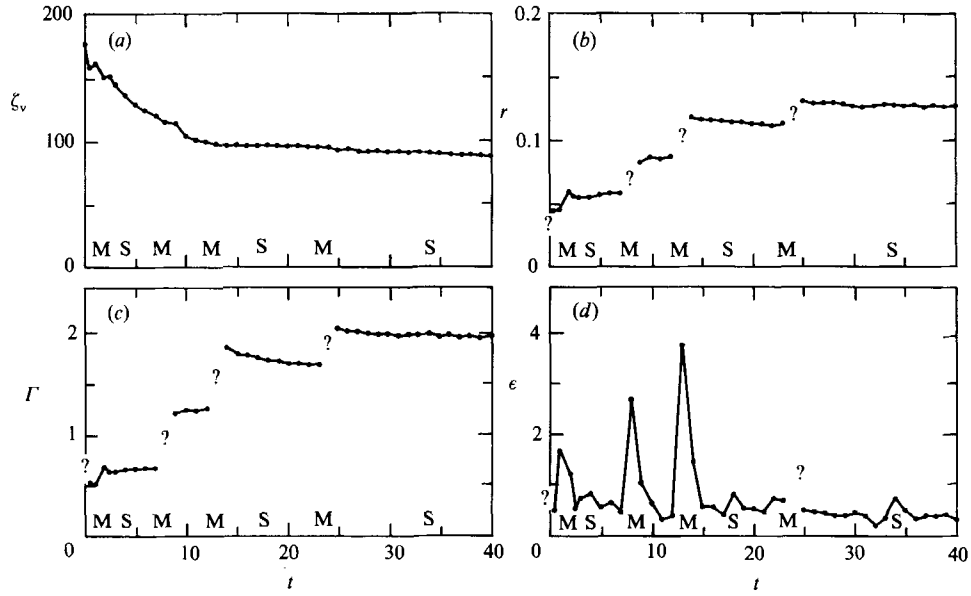

FIGURE 3. Vortex properties of the single vortex in figure 2: (*a*) amplitude ζ_v, (*b*) radius r, (*c*) circulation Γ, and (*d*) ellipticity ϵ. On the time axes are marked the same interaction events as in figure 2. '?' indicates that the property value is missing because the vortex is rejected by the selection procedure (NB some properties are available even for rejected vortices, and which ones depends upon the reason for rejection).

the left-hand-side of (1)) or to the possibility of growth in a vorticity extremum permitted by hyperviscous diffusion; both effects are more likely where vorticity gradients are especially large, and, in my judgement, these non-physical effects are unimportant in the present solution. The straining events show only a modest influence on vortex amplitude here, since, for this vortex, the strain amplitude is never as large as the vorticity in the core, and consequently vorticity gradients are only moderately increased from the axisymmetric configuration. However, one expects enhanced amplitude decay in a strong enough straining event.

Vortex size (figure 3*b*) shows relatively little change except during mergers, when it increases stepwise, as substantial fractions of the areas of the vortex partners combine. Between mergers, the radius usually decreases slightly, to a somewhat greater degree during modest straining events. This tendency is opposite to the effect of diffusion (see the Appendix); it can occur by the casting off of vorticity filaments in the axisymmetrization process during the later phase of a merger, and it can occur through the stripping of weak vorticity patches from the periphery of a vortex due to strain from neighbouring vortices (e.g. Dritschel 1988*b*). Similar behaviour is seen in the vortex circulation,

$$\Gamma = |\sum_V \zeta \, \mathrm{d}s^2|, \tag{18}$$

but to an amplified degree (figure 3*c*). Thus, we conclude that diffusion by itself has relatively little influence on the growth in vortex size, although, of course, it makes an essential contribution to the return to smoothness following straining events.

Vortex deformations are highly variable in time (e.g. ϵ in figure 3*d*): deformation is strain induced, the strain field decays as inverse distance squared away from a vortex of finite circulation, and the nearest neighbour separation distance is highly

variable in vortex motions owing to mutual advection. Overall, vortex deformations decrease with time as average separation distance increases, although we see that substantial averaging is required to educe this behaviour (see figure 10). Sharp peaks in deformation occur during close interactions, most strongly during merger but also during straining events. Other measures of deformation, δ and R, show behaviour similar to ϵ.

6. Vortex properties

Here we examine properties of the population of selected vortices as a whole. The analysis is done for all unit times, $0 \leqslant t \leqslant 40$, plus $t = 0.5$ and 2.5 for better resolution during emergence (the results for $t = 1.5$ were lost by accident and not judged worth the effort of recalculation).

The selection procedure yields N_v vortices from among N_e extrema. The selection ratio N_v/N_e is plotted in figure 4. At $t = 0$ this ratio is quite small, and shortly thereafter, around the time of maximum dissipation hence maximum vorticity deformation, it becomes even smaller, with a value of 0.07. It is reassuring that the selection procedure accepts only a very small fraction of the extrema at early times when coherent vortices are not manifest. On the other hand, it is difficult, if not impossible, to say what the correct fraction should be during the early stages of vortex emergence. Here are two arguments against its being zero: if selection is by any shape criterion, then by chance that shape will occasionally occur in random initial conditions; in the present solution almost all coherent vortices can be traced continuously backwards in time to an initial extremum, so that one can say that vortices are at least latent, and perhaps even nascent, at even the earliest times.

The selection ratio increases with time (figure 4*a*), as the vortices increasingly dominate the vorticity field and thus the solution. The most rapid increase in N_v/N_e occurs just after $t = 3$, which is approximately the time by which the vorticity field outside the vortices has been significantly depleted through cascade and dissipation. At late times the ratio approaches one, which indicates that the selection procedure is correctly accepting almost all strong extrema as vortices (see figure 1*b*). Also at late times time-averaging is required to see the systematic evolution of the selection ratio because $N_e(t)$ is highly variable: vorticity filaments and their associated extrema are intermittently generated at times of close approach and strong mutual straining between vortices. At early times this process is neither so intermittent nor is it the principal reason for ζ extrema.

The selection ratio also increases with vorticity amplitude (figure 4*b*), and this is increasingly so with time. Stronger vortices are better vortices (i.e. have a shape closer to the posited archetype). After vortex emergence, this is principally due to the degree to which the axisymmetrization process can better overcome the deforming influences of an exterior strain field where the vortex amplitude is larger, although it is also true that at $t = 0$ the larger extrema have shapes closer to the archetype as well. Note that even at late times a small fraction of the extrema with weak amplitude are selected; thus, our analysis is not sensitive to the value of $\zeta_{\min}$ except during the period of emergence when there are so many weak extrema.

By reference to figure 4, one can see the difference between the present selection criteria and the simpler threshold criterion (7) (see §3). The two sets of criteria become increasingly similar at late time and large vortex amplitude, but this convergence occurs only gradually and over hundreds of circulation times t_c. For quite substantial time intervals and amplitude ranges, there are many flow

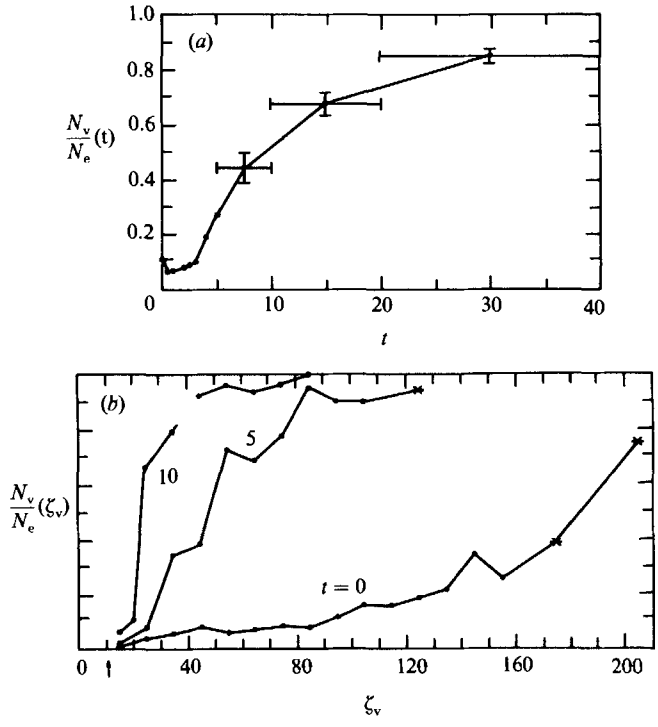

FIGURE 4. Selection ratio for vortices N_v/N_e: (*a*) time evolution and (*b*) dependence on vortex amplitude ζ_v ($=|\zeta_n|$). In (*a*) for $t \leqslant 5$, values are plotted for individual times; for $t > 5$, time-average values are plotted for the indicated intervals with error bars equal to the standard deviation divided by the square root of the number of individual values (at unit times) in the average. For (*b*) the vortex populations are partitioned into ζ_v intervals of either 10 (dots) or 30 (asterisk), the latter where there are relatively few vortices per amplitude interval.

structures that are above the vorticity threshold but do not conform to the coherent vortex shape criterion.

The vortex abundance is shown in figure 5. $N_v(t)$ steadily declines. After the period of emergence, the decline is approximately in the form of a power law, with appreciable scatter due to the intermittency of close encounters, which are occasions of possible vortex destruction through either merger or straining. The best-fit power-law exponent is -0.71 during the interval $5 \leqslant t \leqslant 40$. We can partially interpret this by reference to a simple model for population evolution. If vortex size is small compared with domain size (most stringently, the total area within vortices is small compared to the area of the domain), and if vortex positions are wholly random and mutually uncorrelated, and if the probability of a vortex being destroyed is proportional to the frequency with which any two vortices lie within some critical distance of each other (small compared with the typical separation between vortices), then

$$\frac{\mathrm{d}N_v}{\mathrm{d}t} \propto -N_v^2 \Rightarrow N_v \propto t^{-1}. \tag{19}$$

This is similar to the model by Chandrasekar (1943) for the evolution of colloid particles. Thus, the rate of decline in the vortex population in figure 5 is similar to, but appreciably less steep than, the simple model prediction. Perhaps several model assumptions are falsely simple, but I suspect the most important discrepancy is that

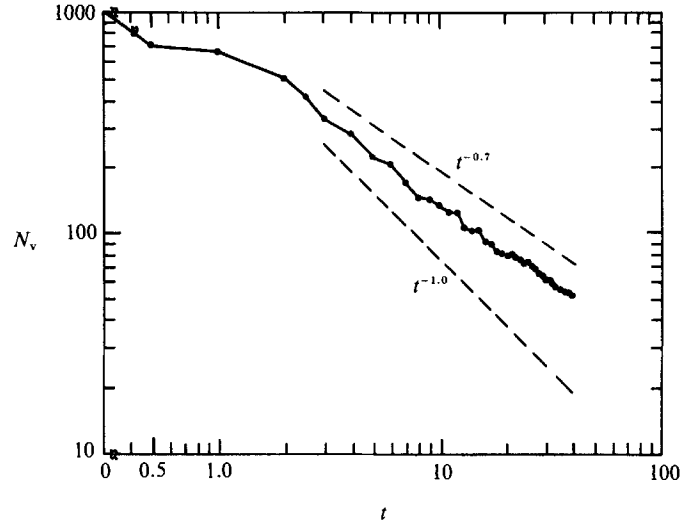

FIGURE 5. Evolution of the vortex population N_v. Comparison lines $\propto t^{-0.7}$ and $t^{-1.0}$ are also plotted.

movement by mutual advection (i.e. point-vortex dynamics) yields close encounters less frequently than random motion (e.g. random walks, as in colloids) because the mutual advection velocity is perpendicular to the separation vector between vortices; however, this conjecture has yet to be demonstrated.

We can define a transformed time $\tau(t)$ which is linear in the geometric progression of $N_v(t)$. If we scale it such that $\Delta\tau = 1$ corresponds to a halving of the vortex population and choose its origin at the onset of the power-law decay regime in figure 5, then

$$\tau(t) = 1.10 \ln t - 0.94 \tag{20}$$

is an accurate fit to the sequence of times, $t = 2.5, 5.7, 13.2, 38.5$, between which three successive halvings of N_v occur. In a solution dominated by coherent vortices, as here, τ is the time for non-conservative evolution of the vortex population and thus of the bulk properties of the solution as a whole (e.g. its spectrum). The form of (20) indicates that this evolution is increasingly slow in the physical time t.

The population distribution with amplitude is shown in figure 6. The distribution of initial extrema is quite broad. The vortex population which emerges from these seeds is also quite broad, although the amplitude range becomes narrower with time owing to hyperviscous dissipation. During the late stages of emergence (e.g. the $t = 2.5$ curve in figure 6), there is a primary population of vortices, whose abundance peaks near $\zeta_v (\equiv |\zeta_n|) = 100$, plus a secondary population of weak vortices, many of which have extrema not present in the initial conditions and which have arisen as filaments and fragments from emerging vortices in close interactions with each other. (This is an exception to the traceability of vortices backwards in time to initial extrema; it is of minor importance in this solution, but it can be more important in others – see §7; it also is a cause for the slower decay rate of $N_v(t)$ before $t \approx 2.5$ in figure 5.) As time proceeds, we see a general decline in both the abundance and amplitude of the main vortex population due to destructive close encounters and hyperviscous diffusion. We also see a preferential destruction of weak vortices, in both the main and secondary populations, due to the decreasing resistance to straining deformations with decreasing vorticity amplitude.

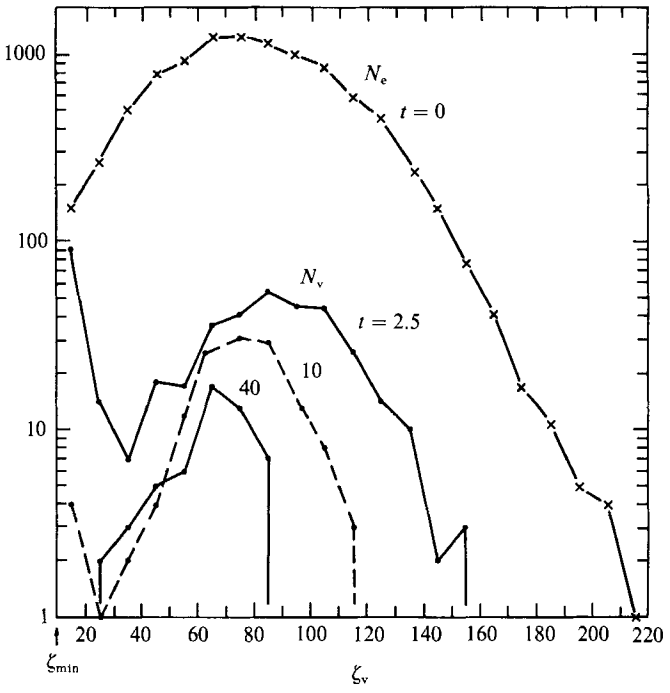

FIGURE 6. Amplitude distributions of initial extrema N_e (×) and selected vortices N_v at subsequent times (●). Vortex amplitudes are grouped into intervals of $\Delta\zeta_v = 10$. Vertical line segments indicate that no vortices exist outside the indicated amplitude interval.

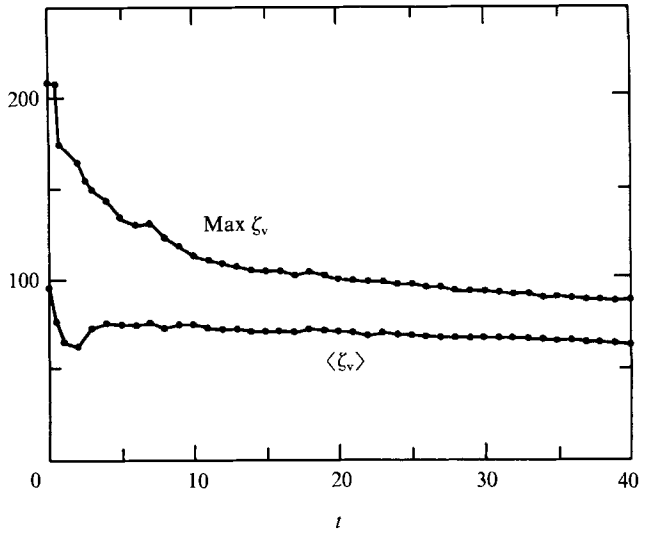

FIGURE 7. The maximum Max ζ_v and average $\langle\zeta_v\rangle$ vortex amplitudes.

The maximum vortex amplitude declines steadily (figure 7). It has a character similar to the amplitude of an individual vortex (figure 3*a*), since it is a composite of individual vortices, each taking its (brief) turn as the strongest. On the other hand, the average amplitude $\langle\zeta_v\rangle$, where $\langle\cdot\rangle$ denotes the average over the population of selected vortices (or some sub-population where specifically stated; e.g. figure 8*b*), declines very much more slowly than max ζ_v after an initial period during emergence

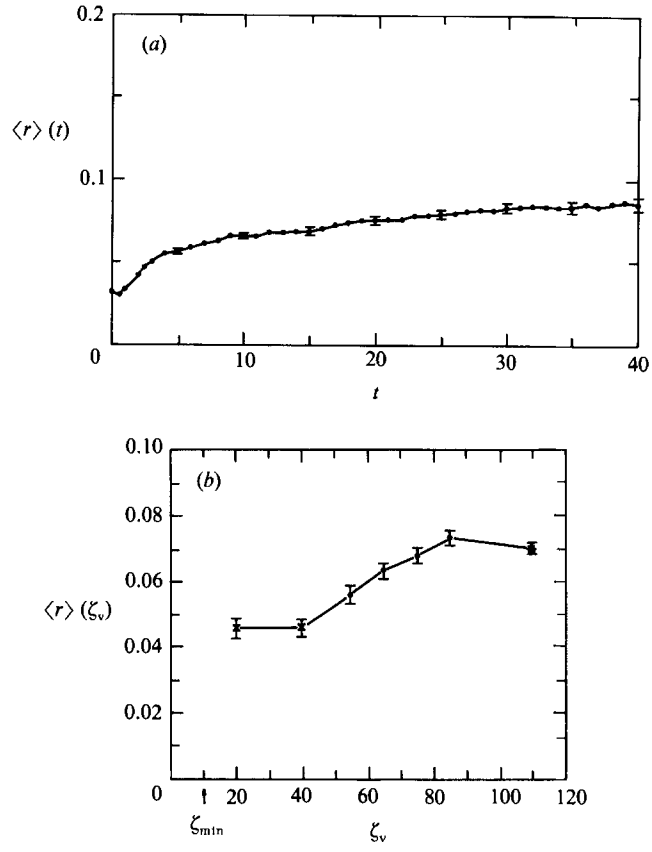

FIGURE 8. Average vortex radius $\langle r \rangle$: (*a*) time evolution, and (*b*) dependence on vortex amplitude. In (*a*) the average is over all vortices at a particular time. In (*b*), the average is over all vortices within the indicated amplitude interval and the time interval $8 \leqslant t \leqslant 12$; ●, $\mu\,\Delta\zeta_v = 10$; ×, 20; *, 40. Error bars are the standard deviation divided by the square root of the number of vortices in the average.

of strong dissipation and creation of weak vortices from interaction fragments. The weak decay of $\langle \zeta_v \rangle$ is a result of the selective destruction of weaker vortices during close interactions, as a balance against the stronger hyperviscous decay of all individual vortices. Both amplitude measures in figure 7 decay substantially more slowly than the square root of the enstrophy (table 1), except at late times. This is because the vorticity within vortices is relatively protected against cascade and dissipation compared with the vorticity outside vortices. The approximate coincidence of the decay rate in all these measures at late times is due to the exhaustion of almost all vorticity except that within the vortices.

Vortex size steadily increases, except near the time of maximum dissipation where strain-induced filamentation dominates (figure 8*a*). Vortex size can grow because of both diffusion and merger. The individual vortex record (figure 3*b*) indicates that the latter is the more important mechanism, even though the pattern of step increases is lost in the population average. The rate of size growth decreases with time as the frequency of close encounters, hence mergers, decreases. Size also increases with amplitude (figure 8*b*; the one exception to monotonicity is sampling error due to the limited number of vortices present). To some degree this relation is a residual bias from the random initial conditions. The shape of $\langle r \rangle$ (ζ_v) changes only slightly with

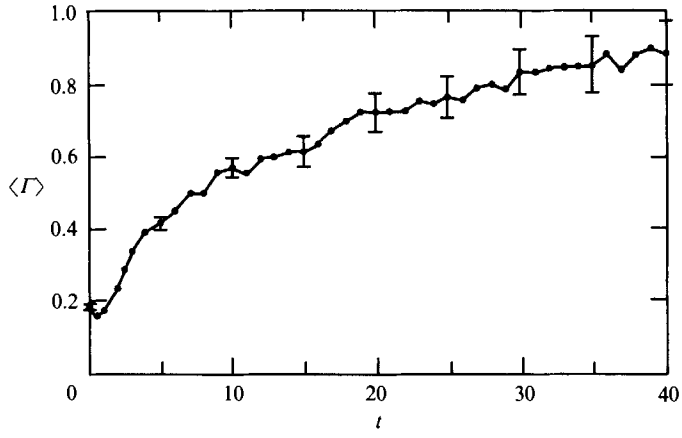

FIGURE 9. Average vortex circulation $\langle \Gamma \rangle$. Error bars are equal to the standard deviation divided by $N_{\mathrm{v}}^{\frac{1}{2}}$.

time until quite late in the evolution (i.e. $t \gtrsim 20$). This is an indication that among the surviving vortices the growth rates in radius are similar for different amplitudes. This in turn is consistent with an amplitude and horizontal-scale independence in the non-viscous dynamical processes. At late times, however, $\langle r \rangle$ (ζ_{v}) steepens considerably; this is because, once weak vortices become relatively rare, the rate of encounter and merger between two weak vortices, yielding a larger weak vortex, becomes quite small compared with encounters and mergers involving at least one strong vortex.

Average vortex circulation also increases with time (figure 9). Its growth ratio for a given time interval is approximately the square of the growth ratio for vortex radius (figure 8*a*). This is characteristic of merger interactions where growth is by accretion, but not of diffusion where Γ and r grow in quite a different relation (see the Appendix). From (18) and figure 8(*b*), it is obvious that $\langle \Gamma \rangle$ is a strongly increasing function of vortex amplitude; hence this is not plotted here.

Each of the properties $\langle \zeta_{\mathrm{v}} \rangle$, $\langle r \rangle$, and $\langle \Gamma \rangle$ also has an approximate power-law form, $\propto t^{\alpha}$, after the initial period of vortex emergence. The best-fit exponents over the interval $5 \leqslant t \leqslant 40$ are, respectively, $\alpha = -0.09$, 0.20, and 0.35. A simple model for inviscid merger of equal vortices which conserves all parcels would predict that $\alpha_{\Gamma} = 2\alpha_r$ and $\alpha_{\zeta} = 0$, which is approximately true for the above exponents. (For unequal vortices, with fractional losses of area and circulation during merger, there is no universal value of α_r/α_{Γ}; so one should not take this model too seriously.) A modest influence of diffusion associated with the strong straining and deformation in mergers would amend the above relations to $\alpha_{\Gamma} \lesssim 2\alpha_r$ and $-\alpha_{\zeta} \gtrsim 0$, since Γ is not altered under diffusion (see the Appendix); these amended relations match very well the above exponents. On the other hand, if the population evolution were only through mergers that are wholly conservative of parcels, the total circulation within vortices, $N_{\mathrm{v}} \langle \Gamma \rangle$, would be constant in time. However, from these power-law fits and (20), we see that $N_{\mathrm{v}} \langle \Gamma \rangle \propto t^{-0.71+0.35} = t^{-0.36} \propto \mathrm{e}^{-0.32\tau}$. Thus, the fractional loss of the circulation contained within the vortices on a population halving time is $1 - \mathrm{e}^{-0.32} = 0.27$, which indicates that the population evolution occurs through some combination of leaky mergers and strain-induced filamentation events.

Shape distortion from axisymmetry decreases both with time (except before the time of maximum dissipation) and with amplitude. This is demonstrated in figure 10

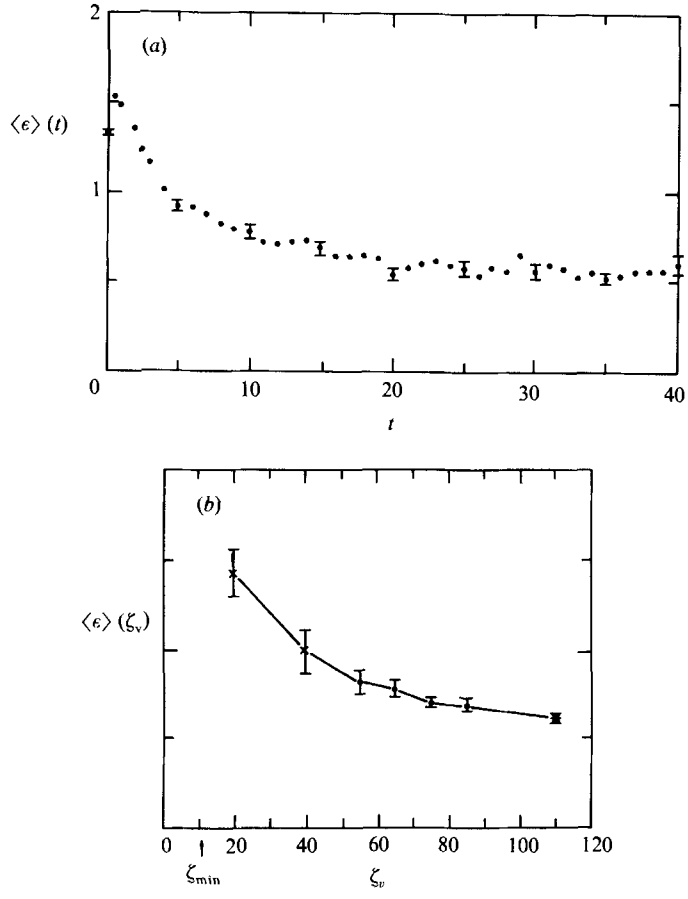

FIGURE 10. Average vortex ellipticity $\langle\epsilon\rangle$ as a function of (*a*) time and (*b*) amplitude. In (*b*), ●, $\Delta\zeta_v = 10$; ×, 20; *, 30. Averaging techniques and error bars are the same as for figure 8.

for ellipticity ϵ, but it is true for the other distortion measures as well. The time dependence $\langle\epsilon(t)\rangle$ is due to decreasing mutual straining among the vortices. In steady solutions of elliptically deformed vortices in a strain field (e.g. Moore & Saffman 1971; Kida 1981), the aspect ratio A exceeds one by an amount approximately proportional to the strain rate divided by the vorticity amplitude. Since strain here is mostly due to distant vortices (except during rare close approaches), we can estimate it as proportional to $\langle\Gamma\rangle$ and inversely proportional to the square of the typical separation distance between vortices, and this distance varies as $N_v^{-\frac{1}{2}}$. Thus, in a power-law fit, as above, we would predict $\alpha_A \approx \alpha_N + \alpha_\Gamma - \alpha_\zeta$ ($= -0.27$ from the above exponents). From (17), $\epsilon = [A(2+A)]^{\frac{1}{2}}$. Thus, at early times when A is typically large, we predict $\alpha_\epsilon \lesssim \alpha_A$, and at late times when A is close to one, we predict $\alpha_\epsilon \gtrsim 0.5\alpha_A$. In a power-law fit to $\langle\epsilon\rangle(t)$, there is indeed a noticeable change to the exponent with time: during $2.5 \leqslant t \leqslant 15$, $\alpha_\epsilon = -0.34$, and during $25 \leqslant t \leqslant 40$, $\alpha_\epsilon = -0.15$, which are in rough correspondence to the predicted values above (i.e. -0.27 and -0.14, respectively). The amplitude dependence $\langle\epsilon(\zeta_v)\rangle$ in figure 10(*b*) is also consequence of deformation's being a decreasing function of the ratio of external strain rate and vortex amplitude. Note that the eventfulness of an individual vortex deformation record (figure 3*d*) is smoothed out in the population record.

Finally, we examine the orthogonal component of vortex shape, i.e. the radial

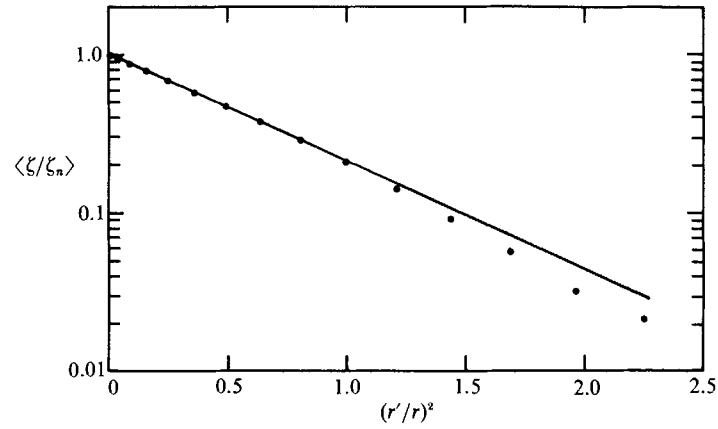

FIGURE 11. Average radial profile for the best-shaped vortices (see text). The straight line is the best-fit Gaussian function, $\exp[-a(r'/r)^2]$, with $a = 1.56$ (also see text).

profiles of the vortices $\zeta(r')$, where r' is the radial coordinate measured from the vortex centre. These profiles are quite variable, as can be seen in figure 1. To educe an average profile, we first do a more stringent selection procedure in order to restrict the inquiry to vortices that have not recently undergone close encounters and have relaxed to axisymmetry. The selection procedure is formally the same as described in §4, except the tolerance parameters are tightened to $r_{\min} = 0.06$, $R_{\max} = 1.25$, $\delta_{\max} = 0.1$, $\epsilon_{\max} = 0.5$. The first of these ensures that at least a modest degree of profile resolution will be achieved, and the other three ensure that departures from axisymmetry will be small. The more stringent selection procedure yields $N_s(t)$ ($\leqslant N_v(t)$) vortices. This number varies little with time after emergence, with a value around 20, as the decline in N_v (figure 5) approximately balances the decline in distortion (figure 10). For each of the stringently selected vortices, an azimuthal average is performed within radial intervals of $\Delta r' = 0.75 \mathrm{d}s = 0.0105$, and then the result is normalized by its extremum ζ_n and interpolated onto a normalized radial coordinate $r'' = r'/r$, on a regular grid with a resolution length of $\Delta r'' = 0.1$.

Even after all this, the resulting profiles show considerable variety. This is consistent with the interpretation that the strongest influences on the shape of an individual vortex are the combination of the (random) initial shape and the shape changes due to synthesis with the particular merger partners encountered. However, a population average of the normalized profiles $\langle(\zeta/\zeta_n)(r'')\rangle$, taken over the stringently selected vortices, does exhibit a preferred shape, and furthermore this shape is approximately independent of time after an initial interval of $\Delta t \approx 10$. The average profile is shown in figure 11, where an additional time average has been done (for the times between 15 and 40 which are divisible by 5) to better expose the preferred shape. This shape is approximately Gaussian, except at large r''. This is made explicit by fitting an unknown radial scale $a^{-\frac{1}{2}}$ so as to minimize the error norm

$$L = \left[\frac{1}{K}\sum_{k=1}^{K}\left[1 - \left\langle \frac{\zeta_n \mathrm{e}^{-ar_k''^2}}{\zeta(r_k'')}\right\rangle\right]^2\right]^{\frac{1}{2}}, \tag{21}$$

where $r_k'' = (k-1)\Delta r''$. We choose $K = 11$ with $r_k'' = 1.0$ (since L increases substantially for larger K) and obtain a quite small minimum value of $L = 0.0109$ for $a^{-\frac{1}{2}} = 0.801$. This fitted Gaussian curve is plotted in figure 11 for comparison with the average profile. The uncertainty in the average profile (standard deviation divided

by the square root of the number of vortices in the average) is about equal to L, which indicates that the profile is indistinguishable from the Gaussian form. At large radius the average profile deviates from Gaussian by being substantially steeper. This feature is interpreted as a consequence of the loss of weak-amplitude, peripheral vorticity in straining interactions with other vortices.

Why is the preferred shape for vortices a Gaussian one? We can interpret this as a consequence of diffusion. Diffusion alone is weak in its influence on the shape of any particular vortex (see above), except perhaps at times of order t_ν much later than those examined here, but its influence is systematic in a way that the more dramatic advective events are not, and thus its effects can be seen in a population average. The Gaussian shape is approached asymptotically in time under radial diffusion; this property is exact for all radii for Newtonian viscous diffusion, and it is approximate for small and intermediate radii for hyperviscous diffusion (see the Appendix). The actual diffusion in coherent vortices, of course, is not axisymmetric and occurs primarily during intermittent events of large straining deformations. Nevertheless, it appears that continuous symmetric diffusion is an apt model for vortex profiles even in the complicated evolution of two-dimensional turbulence. However, a puzzling aspect of this explanation is that the accuracy of a Gaussian fit in figure 11 is slightly better than it is for the asymptotic profile of hyperviscous diffusion (figure 12, Appendix). Perhaps the more complicated real situation makes the particular functional form for the diffusive operator of secondary importance and the net result close to 'classical' diffusion (i.e. the Newtonian form) in turbulent flows where the diffusion is substantially shear-enhanced. In any event, under this interpretation, the elapsed time before the Gaussian profile becomes evident ($\Delta t \approx 10$) is that required for most vortices to have had several close interactions, hence to have experienced significant shear-enhanced diffusion.

7. Summary and discussion

The vortex census selects flow structures based upon the similarity of the local vorticity field to a single-sign, axisymmetric, simply connected distribution surrounding a central extremum of sufficient magnitude. The selection procedure is reasonably successful at discriminating between early times and weak extrema, where there are few coherent vortices, and late times and strong extrema, where almost all extrema are coherent vortices. The properties of the population of selected vortices have broad distributions, which arise through spatially local vortex emergence from the broad-band, random initial conditions. These property distributions evolve in time principally through the dynamical processes of mutual straining and deformation, axisymmetrization, merger, and vorticity diffusion. The evolution is towards fewer, sparser vortices, with the weaker members of the population more likely to be destroyed or absorbed than the stronger ones during a given interval. Among the surviving vortices, the average size and circulation increase (principally during mergers), the amplitude decreases, the deformation from axisymmetry decreases, and the radial profile approaches the Gaussian form within the core region where the vorticity has sufficient magnitude relative to the ambient strain field. Within the vortex population, these properties tend to be well ordered by increasing vortex amplitude: the likelihood of selection increases, the size and circulation increase, and the deformation decreases. Of course, for any individual vortex during any particular interval of strong interaction with other vortices, substantial departures from the population-average behaviour can occur.

Among the previous investigations of vortices in two-dimensional turbulence, Benzi *et al.* (1988) is the one most similar to the present study in its topics. (The maximum Reynolds number and resolution of its solutions are also similar.) There the vortex selection criterion is the simple one of a threshold amplitude (i.e. $\zeta \geqslant \zeta_{\min}$), which is reasonably apt for late times. The ordering variable in analysing the vortex population is radius, in contrast to our preference for amplitude. Their principal hypothesis is that there are aspects of self-similarity with r for the vortices: vortex dynamics are independent of r; $\zeta(r')$ has a universal shape (normalized by amplitude ζ_v and size r, with $\langle\zeta_{\mathrm{v}}\rangle$ nearly independent of r); $N_{\mathrm{v}}(r)$ has a power-law dependence on r; and, consequently, the energy spectrum $E(k)$ has a power-law dependence with an exponent of approximately -4.3.

Our results differ in certain respects from the above, specifically in the non-trivial slope of $\langle r\rangle(\zeta_{\mathrm{v}})$ (figure 8*b*) and the absence of a clear power-law form for either $N_{\mathrm{v}}(r)$ (see figure 6) or $E(k)$. On the other hand, scale- and amplitude-independence of the dynamics are intrinsic properties of (1) and (2) as $k_0 \to \infty$ and $\nu k_0^4 \to 0$, and it seems almost inevitable that an initial energy spectrum of power-law form would yield power-law distributions in the emergent vortex properties, although it is by no means clear that the power-law exponent would always be a universal constant. However, we have found some degree of universality in the population-average vortex shape (figure 11). Furthermore, we have found (but not shown) that the population-average vortex properties in our solution generally have a weaker functional dependence when ordered by size rather than amplitude.

These differences have their origins in the initial conditions, specifically the relation between the initial $E(k)$ and the vortex population which emerges at early time. It seems clear, from examining many solutions, that a broader bandwidth for $E(k)$ yields a broader size range for the emergent vortices and that the shape of $E(k)$, within the wavenumber band where its amplitude is substantial, influences the early-time distributions of N_{v}, ζ_{v}, and r. (This point is also made in the recent paper by Santangelo *et al.* 1989.) The solutions of Benzi *et al.* (1988) have an initial spectrum shape

$$E(k) \propto \frac{k}{\left(1+\left(\frac{k}{k_0}\right)^4\right)}, \tag{22}$$

for a small k_0; this has a much broader bandwidth than (4). A precise and general characterization of the relation between initial conditions and early-time vortex property distributions has not yet been achieved. Nevertheless, we believe that the evolutionary tendencies in the property distributions will exhibit the behaviour shown in this study, over a very broad range of initial conditions, hence of emergent vortex property distributions.

Another unresolved issue is the role of coherent vortex generation through secondary instability of vorticity filaments created by either the enstrophy cascade or as interaction fragments (or filaments) between coherent vortices of larger scale. It seems clear that this process can occur when the cross-filament scale is large compared with the viscous scale and the filament vorticity amplitude is large compared with the ambient strain field. In our solution almost all of the vortices emerge from vorticity extrema in the initial conditions, although some evidence for secondary generation of weak vortices at early times is seen in figure 6. Secondary generation seems to be somewhat more common in a solution with (21) as its initial condition, but still it is not the primary vortex generation mechanism at presently

accessible Reynolds numbers. This issue would best be investigated in even higher resolution solutions, with a very large-scale range between the size of the emergent vortices and the viscous scale.

The National Center for Atmospheric Research is sponsored by the National Science Foundation. I appreciate discussions with Dr Jeffrey Weiss on the subject of vorticity diffusion; in particular, he derived the asymptotic formulae in the Appendix.

Appendix. Vorticity diffusion

Consider an equation for vorticity diffusion:

$$\zeta_t = \mu\nabla^2\zeta - \nu\nabla^2\nabla^2\zeta. \tag{A 1}$$

It contains both Newtonian diffusion, with viscosity μ, and hyperviscous diffusion, as in the barotropic vorticity equation (1). It can be considered either as a linearization of (1) or as its axisymmetric limit, with

$$\zeta = \zeta(r', t) \quad \text{and} \quad \nabla^2 = \frac{1}{r'}\frac{\partial}{\partial r'}\left(r'\frac{\partial}{\partial r'}\right);$$

in either case, advection is trivial.

For $\nu = 0$, a particular solution of (A 1) is

$$\zeta(r', t) = \zeta_0\left(\frac{t_0}{t}\right)\exp\left[\frac{-r'^2}{4\mu t}\right]. \tag{A 2}$$

Its amplitude decreases as $1/t$, and its bulk radius r (as defined in §4: the radius at which the vorticity is a given fraction of its extremum) increases as $t^{\frac{1}{2}}$. Its circulation Γ is time invariant when the vorticity integral spans all radii, $0 \leqslant r' \leqslant \infty$; it is also invariant when the integral spans $0 \leqslant r' \leqslant r$, as in (18). Its normalized profile, when analysed as in figure 11, is also time invariant, and it is a Gaussian function of r'.

The solution (A 2) is asymptotically approached in time for general initial conditions of a vorticity-monopole type, and in this sense it is the favoured vortex profile under the influence of Newtonian diffusion. This result is easily derived by making Bessel and Fourier transforms of (A 1) in r' and θ, solving the resulting temporal ODE, and regrouping the solution as a series in powers of $t^{-\frac{1}{2}}$.

For hyperviscous diffusion (i.e. with $\mu = 0$ in (A 1)), the analogue to (A 2) does not have such a simple expression. From numerical integrations of (A 1) with initial conditions of a vorticity-monopole type, it is clear that the amplitude decreases and the bulk radius grows with time here as well, but they do so with less steep functional dependences on time, compared to the Newtonian solution (A 2). The circulation Γ, integrated over $0 \leqslant r' \leqslant r$, is not time invariant; it is slowly growing with time, but at a rate much less than that of r^2. The leading-order asymptotic profile, derived as described above, can be expressed as a power series in a similarity variable $\xi = r'^2/4(\nu t)^{\frac{1}{2}}$; viz.

$$\zeta(r', t) = \zeta_0\left(\frac{t_0}{t}\right)^{\frac{1}{2}} F(\xi), \tag{A 3a}$$

where

$$F(\xi) = \pi^{-\frac{1}{2}}\sum_{m=0}^{\infty}\frac{(-1)^m\Gamma\left(\frac{m+1}{2}\right)}{\Gamma(m+1)^2}\xi^m, \tag{A 3b}$$

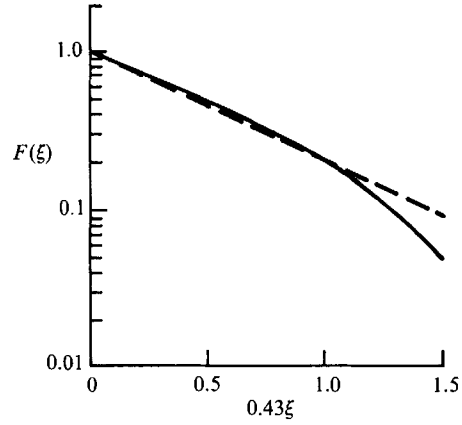

FIGURE 12. Asymptotic profile for hyperviscous vorticity diffusion (A 3). The dashed line represents a Gaussian function of radius, $e^{-0.43\xi}$, such that the function values are 1.0 and 0.2 at $0.43\xi = 0$ and 1.

where here only Γ denotes the well-known Gamma function and not circulation. The solution (A 3) has its amplitude decrease as $t^{-\frac{1}{2}}$ and its size grow as $t^{\frac{1}{4}}$. Its normalized radial profile is again time-invariant: it is $F(\xi)$, with $\xi \propto (r'/r)^2$. $F(\xi)$ is plotted in figure 12. It is close to the Gaussian form for ξ values up to a little beyond 2. This range approximately spans the interval from the origin to $\xi = 2.33$, where $F = 0.2$ $(= \Delta)$. For easier comparison with figure 11, the abscissa in figure 12 is $\xi/2.33 = 0.43\xi$.

REFERENCES

BABIANO, A., BASDEVANT, C., LEGRAS, B. & SADOURNY, R. 1987 Vorticity and passive-scalar dynamics in two-dimensional turbulence. *J. Fluid Mech.* **183**, 379–397.

BASDEVANT, C., LEGRAS, B., SADOURNY, R. & BELAND, M. 1981 A study of barotropic model flows: intermittency, waves, and predictability. *J. Atmos. Sci.* **38**, 2305–2326.

BATCHELOR, G. 1967 *Introduction to Fluid Dynamics.* Cambridge University Press, 615 pp.

BENZI, R., PALADIN, G., PATARNELLO, S., SANTANGELO, P. & VULPIANI, A. 1986 Intermittency and coherent structures in two-dimensional turbulence. *J. Phys.* A: *Math. Gen.* **19**, 3771–3784.

BENZI, R., PATARNELLO, S. & SANTANGELO, P. 1988 Self-similar coherent structures in two-dimensional decaying turbulence. *J. Phys.* A: *Math. Gen.* **21**, 1221–1237.

BRACHET, M., MENEGUZZI, M., POLITANO, H. & SULEM, P. 1988 The dynamics of freely decaying two-dimensional turbulence. *J. Fluid Mech.* **194**, 333–349.

BRACHET, M., MENEGUZZI, M. & SULEM, P. 1986 Small-scale dynamics of the high Reynolds number two-dimensional turbulence. *Phys. Rev. Lett.* **57**, 683–686.

CHANDRASEKAR, S. 1943 Stochastic problems in physics and astronomy. *Rev. Mod. Phys.* **15**, 1–89.

CHRISTIANSEN, J. & ZABUSKY, N. 1973 Instability, coalescence, and fission of finite-area vortex structures. *J. Fluid Mech.* **61**, 219–243.

DRITSCHEL, D. 1988*a* Nonlinear stability bounds for inviscid, two-dimensional, parallel or circular flows with monotonic vorticity, and the analogous three-dimensional quasi-geostrophic flows. *J. Fluid Mech.* **191**, 575–581.

DRITSCHEL, D. 1988*b* Strain-induced vortex stripping. In *Mathematical Aspects of Vortex Dynamics* (ed. R. E. Caflisch), pp. 107–119. Soc. Ind. Appl. Math.

FORNBERG, B. 1978 A numerical study of 2D turbulence. *J. Comput. Phys.* **25**, 1–31.

HERRING, J. & MCWILLIAMS, J. 1985 Comparison of direct numerical simulation of two-dimensional turbulence with two-point closure: the effects of intermittency. *J. Fluid Mech.* **153**, 229–242.

KIDA, S. 1981 Motion of an elliptic vortex in a uniform shear flow. *J. Phys. Soc. Japan* **50**, 3517–3520.

LAMB, H. 1932 *Hydrodynamics.* Dover, 738 pp.

LEITH, C. 1984 Minimum enstrophy vortices. *Phys. Fluids* **27**, 1388–1395.

LESIEUR, M. 1987 *Turbulence in Fluids.* Martinus Nijhoff, 286 pp.

LILLY, D. 1969 Numerical simulation of two-dimensional turbulence. *Phys. Fluids Suppl. II*, 240–249.

MCWILLIAMS, J. 1983 On the relevance of two-dimensional turbulence to geophysical fluid motions. *J. Méc., Num. Spéc.*, pp. 83–97.

MCWILLIAMS, J. 1984 The emergence of isolated coherent vortices in turbulent flow. *J. Fluid Mech.* **146**, 21–43.

MCWILLIAMS, J. 1990*a* Geostrophic vortices. In *Proc. Intl School of Physics Enrico Fermi.* Italian Physical Society (in press).

MCWILLIAMS, J. 1990*b* A demonstration of the suppression of turbulent cascades by coherent vortices in two-dimensional turbulence. *Phys. Fluids* A **2**, 547–552.

MELANDER, M., MCWILLIAMS, J. & ZABUSKY, N. 1987 Axisymmetrization and vorticity-gradient intensification of an isolated two-dimensional vortex through filamentation. *J. Fluid Mech.* **178**, 137–159.

MOORE, D. & SAFFMAN, P. 1971 Structure of a line vortex in an imposed strain. In *Aircraft Turbulence and its Detection*, pp. 339–354. Plenum.

ORSZAG, S. 1971 Numerical simulation of incompressible flows within simple boundaries. I. Galerkin (spectral) representations. *Stud. Appl. Maths.* **L**, 293–328.

RAYLEIGH, LORD 1880 On the stability, or instability of certain fluid motions. *Proc. Lond. Math. Soc.* **11**, 57–70.

SANTANGELO, P., BENZI, R. & LEGRAS, B. 1989 The generation of vortices in high-resolution, two-dimensional, decaying turbulence and the influence of initial conditions on the breaking of self-similarity. *Phys. Fluids* A **1**, 1027–1034.

WEISS, J. 1981 The dynamics of enstrophy transfer in two-dimensional hydrodynamics. *La Jolla Inst. Tech. Rep.* LJI-TN-81-121.